International Journal of Material Forming (2021) 14:499–506
https://doi.org/10.1007/s12289-019-01527-x

ORIGINAL RESEARCH

A forming time estimator of superplastic free bulge tests based on dimensional analysis

L. García-Barrachina[1] · A. J. Gámez[1]

Received: 1 April 2019 / Accepted: 17 November 2019 / Published online: 3 January 2020

Abstract
Dimensional analysis is performed as a method to evaluate the characteristics of superplastic forming processes. The analysis is focused on the forming time results from superplastic free bulge tests so that an estimator for the forming time is obtained based on dimensionless parameters. The dimensional analysis is performed by applying the normalisation to the dynamic equations and their corresponding boundary conditions, from which five dimensionless parameters are obtained. Particular conditions of the tests allow to reduce the parameters to two. This preliminary study of the applicability of the dimensional analysis on superplastic forming processes will guide for further steps in which this technique may help during the initial stages of the process layout.

Keywords Bulge · Test · Dimensional · Analysis · Superplastic

Introduction

Superplastic forming (SPF) is a manufacturing process that takes advantage of the superplastic characteristic that certain materials exhibit at specific ranges of temperature, strain and strain rates [1]. During a standard SPF, a blank fine grained sheet of material is placed between an upper and a lower die. The system is sealed along the perimeter of the blank. In case the material is sensitive to oxidation, air is replaced by an inert gas, i.e. argon. Once the atmosphere is replaced, heating is applied and the material is guided to its working temperature. Also, a pressure-control system is required to ensure that the strain-rate remains within the necessary range [2]. Thus, three main features are necessary to manage the SPF: an external heating source that reaches and keeps the temperature within the specific range, a piping system that allows replacing the air by an inert atmosphere and a pressure-control system that ensures to keep the strain-rate near a target.

Materials like AA5083 or Ti-6Al-4V are commonly used in automotive and aerospace industry [3, 4]. This latter alloy is chosen by its high corrosion resistance and the high mechanical performances at high temperatures. These two properties are specially important for leading-edge wings and inlet engine regions where air friction becomes significant. Moreover, these parts present generally complex shapes, [5], and are expected to increase its complexity over the years since CAD and CAE tools are progressing. SPF has proven to be an adequate manufacturing process for laminar complex shapes. In the case of the military aerospace industry, the percentage of Ti-6Al-4V used is increasing as well as the use of SPF for certain pieces, being applied even to fuselage parts or complete tail planes [6].

The superplastic behaviour is usually modelled by the Norton-Hoff power law, relating the Cauchy stress, σ, to the strain rate, $\dot{\varepsilon}$, through a strain rate sensitivity index m and a constant K [7].

$$\sigma = K\dot{\varepsilon}^m \tag{1}$$

This model is based on the assumption that K and m are strain-rate independent constants and that neither hardening, softening nor damage accumulation are taken into account. Different constitutive model proposals have tried to overcome these issues with more complex equations that can track the hardening, softening or the damage occurring at the microstructure as well as the change in grain size during the process [1, 8]. Our analysis can be easily extended to these cases.

✉ L. García-Barrachina
luis.barrachina@uca.es

[1] Department Mechanical Engineering and Industrial Design, School of Engineering, University of Cadiz, Av. Universidad de Cádiz, 10, Puerto Real, Cádiz E-11519, Spain

The standard E2448-11 [9] establishes the method, i.e. shape sample and load profile to test, via uniaxial samples, the materials and obtain the superplastic properties depending on strain, strain-rate and temperature.

Other standards like E2712-15 [10] are also applied to SPF and allow to evaluate whether a blank sheet is able to form up to a certain depth without breaking. Unfortunately, this standard have been used successfully only with aluminum alloys and the application to titanium alloys must be verified at first. Similar to E2712-15, this article will focus on the study of free-bulge forming (FBF) tests. Unlike E2712-15, the tests are considered completed when the blank-sheet forms a complete circular dome.

Free-Bulge Forming (FBF) [11] has been extensively used as a test procedure for superplastic manufacturing process during the last decade. Several purposes have usually been intended: to be a SPF-parameter evaluator in order to find the best conditions in terms of temperature and forming pressure; to give the best compromise between the alloy formability and the forming time, [12]; to constitute an alternative superplastic material characterisation method, [13–19]; to become a way to evaluate some proposed material constitutive equations [20–22]; and also as a method to study the micro structure behaviour [23].

In recent years, much attention has been paid to FBF as a particular biaxial test thanks to its high versatility. Compared to uniaxial tests, FBF tests provide material information by using an easier shape of the blank, in the sense that requires less pre-processing machining. Moreover, FBF tests are generally easier to perform compared to uniaxial tests since they apply an easier load profile (constant pressure) while uniaxial tests must follow a specific load profile that controls the strain and the strain-rate of the sample during the test. Although uniaxial test is the current standard for analysing superplastic material behaviour and it is well accepted by the industry, a big effort is been doing by researchers in order to deeply understand the applicability of biaxial tests through FBF.

On the other hand, Dimensional Analysis (DA) [11, 24] has been proved as a useful technique in several scientific fields, such as fluid dynamics or thermodynamics. Thanks to DA, different tests can be compared using the minimum number of variables through dimensionless parameters. In other words, the analysis of a certain process can be performed by studying dimensionless variables. This reduces the number of dimensions, and so the tests that are needed to analyse the whole process.

However, DA is not as used in manufacturing process as in the aforementioned disciplines, although it gives the chance not only to test in down-scale dimensions, but also to apply different materials as long as the similarity of the geometry, process and material is fulfilled. That means that a real process, e.g., of a titanium alloy, could be tested in a down-scaled sample and in a equivalent material (similar m) as long as the dimensionless parameters are equal. Some works have used tools from DA, though not in a systematic way [7, 25]. In this work, the great potentiality of DA as a tool to support the initial stages of the process layout is shown, by performing a general analysis from first principles to obtain a forming time estimator that is compared with theoretical and experimental results.

Formulation

Dimensional analysis

FBF consists on the deformation of a circular blank-sheet that is let to expand freely due to a difference of pressure between the two faces. The die containing the sheet is designed in order to minimise the contact with the blank during the test. Thus, the only contact is located at the entry radius, necessary to minimise the stress concentration.

Figure 1 shows a basic scheme of a FBF test, in which the blank is placed over a cylindrical die of radius l_o. At the initial time ($t = 0$) the blank remains flat. As the external pressure goes to q_o, the height at the center point starts to change with time, reaching the target when the circular dome is formed, i.e. $h = l_o$. This is called the forming time, t_o.

The SPF process applied to FBF can be solved using the Cauchy and the continuity equation [11]. A constitutive equation describing the material behaviour and the corresponding boundary equations is also needed. Let Ω be the volume and Γ the boundaries of the body to study. Assuming, as usual, an incompressible behaviour of the material, the density ρ remains constant during the process. This assumption can be made unless the volume fraction of cavities, that depends on the strain and strain-rate, becomes significant [26]. Since the strain-rate of the analysed tests are in the range of typical superplastic applications and the final strain are in the order of 0.5, the density is assumed to be constant during the process. Thus, the continuity equation in its differential form is

$$\nabla \cdot \mathbf{v} = 0 \tag{2}$$

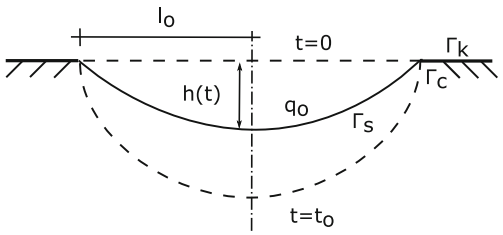

Fig. 1 Geometrical scheme of FBF for dimensional analysis

where $\mathbf{v}$ is the velocity vector at each point. The lagrangian formulation of the Cauchy equation is written in terms of unit of volume

$$\rho\left(\frac{d\mathbf{v}}{dt} - F_i\right) = \frac{\partial \sigma_{ij}}{\partial x_j} \tag{3}$$

where F_i represents the body forces in acceleration units, and the σ_{ij} are the Cauchy stress tensor elements.

The constitutive equation is formulated in its scalar form, i.e. the equivalent stress, σ_e, is calculated as a function of the deformation history, s, and the equivalent strain-rate, $\dot{\varepsilon}_e$.

$$\sigma_e = \Phi\left(s, \dot{\varepsilon}_e\right) \tag{4}$$

The boundary value problem is completed with the conditions over Γ. The external surface is divided in three different regions depending on the kind of boundary condition applied to it,

$$\Gamma = \Gamma_k \cup \Gamma_s \cup \Gamma_c \tag{5}$$

Dirichlet or kinematic boundary conditions apply at Γ_k. This region is located along the perimeter of the blank x_b where a zero-displacement condition, due to the sealing clamp, is assumed.

$$\Gamma_k \subset \Gamma : \mathbf{v} = \mathbf{f}(x_b, t) \tag{6}$$

Neumman or dynamic conditions apply at Γ_s and refer to the external pressure,

$$\Gamma_s \subset \Gamma : \sigma_{ij} n_j = q_j \tag{7}$$

Finally, mixed boundary conditions are located at Γ_c and refer to a sliding motion, $\Delta\mathbf{w}$, between the blank and the die, related to the contact pressure, σ_N, and the friction coefficient, υ. This region is located mainly at the entry radius.

$$\Gamma_c \subset \Gamma : \tau = \phi(\sigma_N, \Delta\mathbf{w}, \upsilon) \tag{8}$$

A set of characteristic values of the problem are chosen in order to normalise the equations. The die radius, l_o, and the forming time, t_o, are set as characteristic length and time, respectively. Also, a characteristic strain-rate, $\dot{\varepsilon}_o$, and stress, σ_o, are used. The meaning of these values will be explained later.

Defining the dimensionless velocity, ν , as,

$$\nu = \frac{t_o}{l_o}\mathbf{v} \tag{9}$$

the continuity equation can be rewritten as,

$$\nabla \cdot \nu = 0 \tag{10}$$

This normalised equation does not provide any dimensionless parameter.

Defining τ, π_{ij}, λ_j and η_i as the normalised variables of time, stress, length and mass forces respectively, the normalised equilibrium equation reads,

$$\frac{d\nu_i}{d\tau} = \left(\frac{\sigma_o}{\rho v_o^2}\right)\frac{\partial \pi_{ij}}{\partial \lambda_j} + \left(\frac{l_o g_o}{v_o^2}\right)\eta_i \tag{11}$$

and two dimensionless parameters, κ_1 and κ_2, can be defined,

$$\kappa_1 = \frac{\sigma_o}{\rho v_o^2} \quad ; \quad \kappa_2 = \frac{l_o g_o}{v_o^2} \tag{12}$$

κ_1 represents the stress forces to inertial forces ratio, while κ_2 compares the gravitational and the inertial forces. Therefore, higher values than 1 of κ_1 implies that stress forces are higher than inertial forces.

A third dimensionless parameter, κ_3, comes out from the constitutive equation

$$\sigma_e = \Phi\left(s, \frac{v_o}{\dot{\varepsilon}_o l_o}\dot{\varepsilon}_e\right) \tag{13}$$

$$\kappa_3 = \frac{\dot{\varepsilon}_o l_o}{v_o} \tag{14}$$

Two additional dimensionless parameters emerge from the mixed and dynamic conditions. Thus, κ_4 and κ_5 are, respectively, the friction coefficient and the external pressure to characteristic stress ratio.

$$\kappa_4 = \upsilon \quad ; \quad \kappa_5 = \frac{q_o}{\sigma_o} \tag{15}$$

This five parameters can also be obtained by combining the five independent Π-groups obtained by direct application of the Buckingham π theorem [27].

Analytical approach

A broad range of strategies have been used to analytically capture the forming evolution on free-bulge tests. Detailed formulation can be found in [7, 13, 28–31]. Here, we adopt an approach based on [30] to compare with experimental results. The following assumptions are employed in the analysis:

- the material is isotropic and only develops a plastic behaviour. Although the anisotropy have been study in magnesium or titanium alloys [21, 32], its effect in the planar behaviour has been reported insignificant [33].
- K and m paramenters are material constant independent of strain-rate. The characteristics of the constant-pressure FBF let to consider that the test will develop in a narrow range of the strain rates, so that the sigmoidal variation of the flow stress can be simplified,
- the volume remains constant as was explained in the last subsection

– the thickness is equally distributed along any meridian following the Jovane model [7],
– the sheet can be shaped as a part of a sphere subject to a constant internal pressure,
– the sheet is clamped at the periphery.

The incompressibility condition can be written as:

$$\dot{\varepsilon}_m + \dot{\varepsilon}_t + \dot{\varepsilon}_s = 0 \tag{16}$$

where $\dot{\varepsilon}_m$, $\dot{\varepsilon}_t$ and $\dot{\varepsilon}_s$ corresponds to the meridian, circumferential and thickness strain-rate respectively. From symmetry, $\dot{\varepsilon}_m = \dot{\varepsilon}_t = -0.5\dot{\varepsilon}_s$. Therefore, the thickness strain can be calculated as

$$\varepsilon_s = \ln\left(\frac{s}{s_o}\right) \tag{17}$$

According to [30], the thickness ratio can be written in terms of the angle α, see Fig. 2, assuming that the thickness is equally distributed along the sheet.

$$\frac{s}{s_o} = \left(\frac{\sin\alpha}{\alpha}\right)^2 \tag{18}$$

Thus, the thickness strain-rate can be written in terms of the dimensionless height H, defined as the height to characteristic length ratio, or in terms of the angle α,

$$\dot{\varepsilon}_s(t) = 2\dot{\alpha}\left(\frac{1}{\alpha} - \cot\alpha\right) = \frac{2H\dot{H}}{1+H^2} \tag{19}$$

where both variables are related as

$$\sin\alpha = \frac{2H}{1+H^2} \tag{20}$$

In addition, the equilibrium equation states that

$$\sigma = \frac{q_o r}{2s} \tag{21}$$

Substituting (19) and (1) into (21) and considering that $l_o = r\sin\alpha$, for a constant pressure test, one can obtain that

$$q_o = const = \left(\frac{2s_o}{l_o}\right) K \left(\frac{\sin^3\alpha}{\alpha^2}\right)\left[2\dot{\alpha}\left(\frac{1}{\alpha} - \cot\alpha\right)\right]^m \tag{22}$$

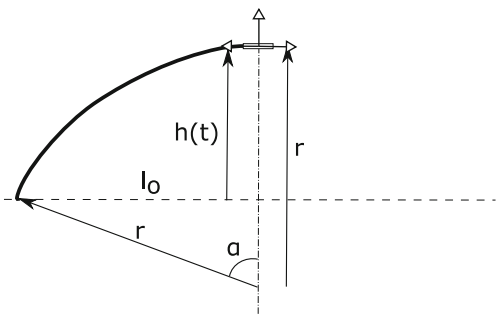

Fig. 2 Geometrical scheme of FBF for analytical approach

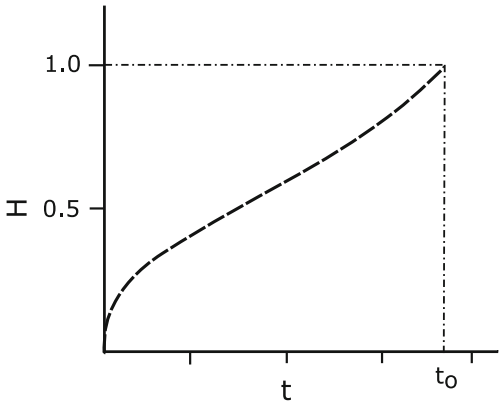

Fig. 3 Characteristic adimensional height (H) evolution during a constant-pressure FBF test

being that a first order ordinary differential equation for the unknown function $\alpha(t)$. Integrating is possible to obtain an implicit equation of $\alpha(t)$

$$t = 2I_m(\alpha)\sqrt[m]{\frac{2K}{q_o AR}} \tag{23}$$

where the Aspect Ratio (AR) has been defined as the die radius to sheet thickness ratio, and I_m can be calculated as

$$I_m(\alpha) = \int_0^\alpha \left[\left(\frac{\sin^3\alpha}{\alpha^2}\right)\right]^{1/m}\left(\frac{1}{\alpha} - \cot\alpha\right)d\alpha \tag{24}$$

Methodology

The analysis starts from an experimental curve that traced the time evolution of the center dome height for a constant-pressure FBF until it reached the forming time. This height-time curve (h, t) was later transformed into a normalised height-time curve (H, t), Fig. 3.

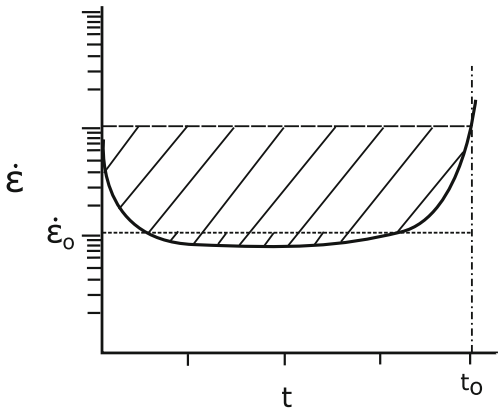

Fig. 4 Characteristic strain-rate ($\dot{\varepsilon}$) evolution at the apex-dome during a constant-pressure FBF test

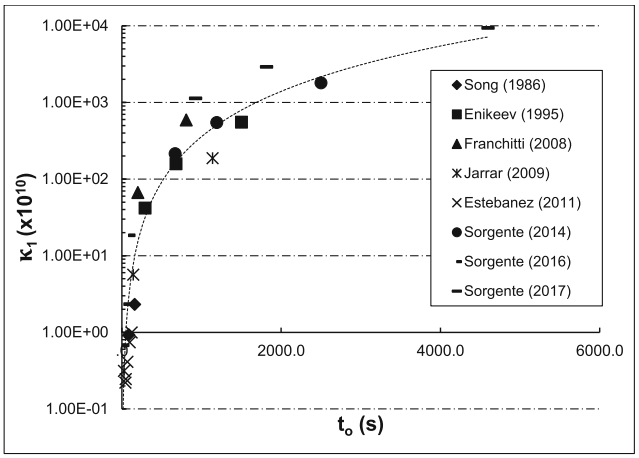

Fig. 5 Correlation between κ_1 and the forming time. The dotted line represents the power law function

H is in the range of [0,1], where $H = 0$ corresponds to the undeformed configuration and $H = 1$ corresponds to the completed circular dome. Therefore, following the dimensionless height at the apex dome during the forming process, an abrupt transient state occurs during the first seconds, which seems to be influenced by the near-zero stiffness of the blank in its initial flat configuration. After this first state, a steady state is reached, appearing a nearly constant velocity at the center of the dome. The (H, t) curve allows us to calculate the strain-rate at the center point, according to [7], using (19)

Figure 4 shows a typical behaviour of the apex-dome strain-rate during a constant-pressure FBF process. Despite of being a pressure-controlled process, a nearly constant strain-rate $\dot{\varepsilon}_o$ is found in the course of the forming time. The characteristic strain-rate was defined, as a dimensionless measurement, from Fig. 4 as the 2nd percentile of the strain rate during the forming time, which approaches the slope from Fig. 3.

Thus, obtaining σ_o is straightforward using $\dot{\varepsilon}_o$ and (1). With this last value, the computation of the dimensionless parameters is completed for each experiment.

A first analysis of the five dimensionless parameters let us reduce the study to three of them. First, under SPF conditions the deformation forces are much higher than the gravitational ones. Therefore, κ_2 can be neglected from the

Table 1 Data

Author (Year)	Material (K, m)	AR	Temp. (°C)	q_o (MPa)	$\dot{\varepsilon}_o$ (s^{-1})	t_o (s)	δt (s)	ϵ_r(%)
Song [34]	ZnAl22 (87, 0.35)	25	270	0.4	0.0015	365	73	20.0
				0.6	0.0032	160	31	19.8
				0.8	0.0060	87	17	20.2
Enikeev [30]	Ti6Al4V (410, 0.43)	35	900	0.5	0.00037	1500	326	21.8
				0.7	0.0008	678	144	21.3
				1.0	0.0018	291	61	20.8
Franchitti [19]	AZ31 (136.6, 0.457)	35	520	0.16	0.00069	809	228	28.1
				0.29	0.0026	200	58	28.9
Jarrar [22]	AA5083 (430, 0.5)	41.7	450	0.29	0.0005	1138	271	23.8
				0.56	0.0037	142	33	23.1
				0.90	0.020	26	6	21.3
Estébanez [35]	PbSn60 (36.9, 0.364)	100	50	0.06	0.0041	122	30	24.6
				0.07	0.0058	99	19	19.6
				0.08	0.0084	69	13	19.2
				0.09	0.012	50	10	19.0
				0.10	0.013	45	9	19.4
Sorgente [17]	Alnovi-U (248.2, 0.5)	16.7	500	0.3	0.00022	2499	606	24.2
				0.4	0.00043	1189	303	25.5
				0.5	0.00079	668	158	23.7
Sorgente [12]	AZ31 (195, 0.457)	30	450	0.75	0.0085	87	21	24.1
				1.00	0.017	26	11	41.3
				1.25	0.036	12	6	53.8
Sorgente [36]	Ti6Al4V-ELI (5229, 0.703)	22.5	850	0.50	0.00014	4597	1897	41.3
				1.00	0.00032	1815	749	41.2
				1.25	0.00061	924	372	40.2

normalised Cauchy equation. Results showed that κ_2 was usually four orders of magnitude lower than κ_1. Moreover, κ_4 was also discarded from the study because, in our experimental setup, most of the blank sheet did not have any contact with the die, being limited this contact to the entry radius region.

Results and discussions

A total of 25 independent FBF tests were analysed [12, 17, 19, 22, 30, 34–36]. The tests were performed on lead, zinc, magnesium, aluminium, and titanium alloys within an AR range between 16.7 and 100 and within a thickness range between 0.3 and 2 mm. Table 1 summarizes the analysed tests set.

The analysis was focused on the study of the forming time, being that one of the most characteristic outputs defining the SPF process as they are the thickness distribution or the forming energy. However, the study of the height evolution during the process is usually the most common analysed output within the literature.

κ_1 as a function of t_o

Figure 5 shows the correlation between the forming time and the first dimensionless paramenter κ_1, representing the stress forces to inertial forces ratio. From the normalised Cauchy equation (11) the forming time is related to the two first dimensionless parameters. As it was previously mentioned, the second dimensionless parameter κ_2 can be neglected from the study. Thus, from Eq. 12, κ_1 as a function of forming time can be expressed analytically.

$$\kappa_1(t_o) = \frac{\sigma_o}{\rho v_o^2} = \frac{\sigma_o}{\rho l_o^2} t_o^2 \tag{25}$$

Despite of the heterogeneity of the tests depicted in Table 1, a potential law can be shown as a correlation law between the forming time, t_o, and κ_1, see Fig. 5, that matches with

$$\kappa_1 = (5.23 \cdot 10^6) \times t_o^2 \tag{26}$$

It is noteworthy that, even at quite fast processes, say lower than 20 seconds, the stress forces are significantly higher than inertial forces. Finally, using (26), Eq. 11 remains

$$\frac{dv_i}{d\tau} \approx (5.23 \cdot 10^6) \times t_o^2 \frac{\partial \pi_{ij}}{\partial \lambda_j} \tag{27}$$

κ_5 as a function of *AR*

Figure 6 shows the correlation between the characteristic strain rate and the forming time t_o. In that sense, the definition of the characteristic strain rate proposed in the Methodology section let us get a match between this value and the forming time as a process output.

$$\dot{\varepsilon}_o \approx \frac{1}{2t_o} \tag{28}$$

In addition, this last expression let us understand κ_5 as a dimensional parameter related to the forming time

$$\kappa_5 = \frac{q_o}{\sigma_o(\dot{\varepsilon}_o)} = \frac{q_o}{K\dot{\varepsilon}_o^m} = \frac{q_o}{K}(2t_o)^m \tag{29}$$

Furthermore, an experimental study of κ_5 for the bunch of tests on Table 1 shows that this dimensionless parameter is strongly dependent on the test geometrical characteristic represented by the AR, Fig. 7. This relationship can be expressed approximately as

$$\kappa_5 \approx \frac{1.17}{AR} \tag{30}$$

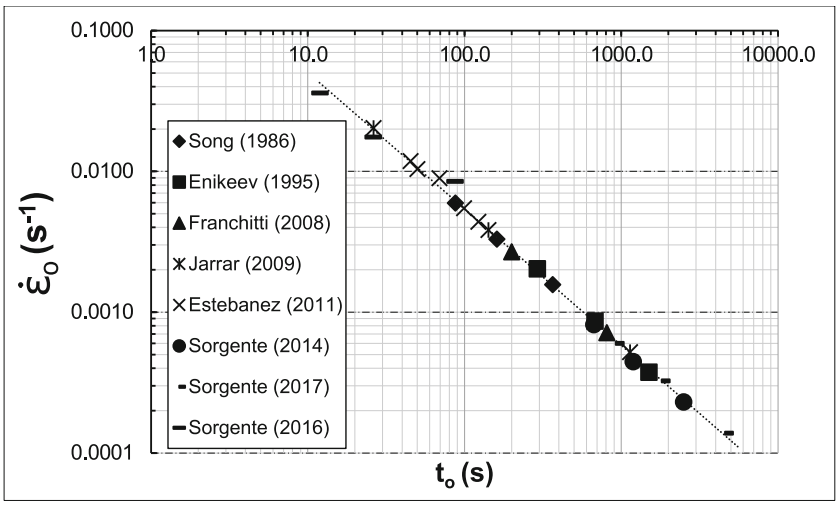

Fig. 6 Correlation between forming time and $\dot{\varepsilon}_o$

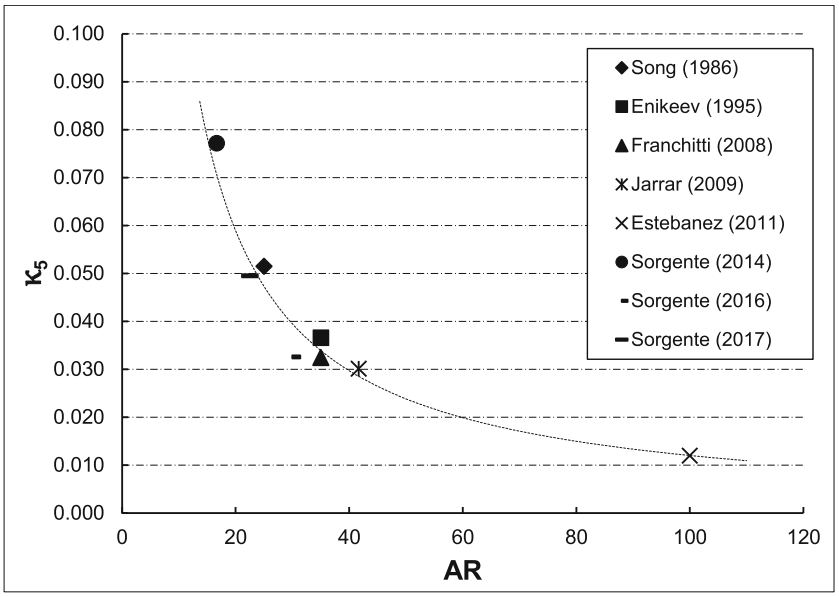

Fig. 7 Correlation between κ_5 and the AR. Placed symbols are calculated as the mean value among all the tests for each article

Applying the material parameters, K and m, and using (29) and (30) the forming time can be estimated as

$$t_o \approx 0.5 \sqrt[m]{\frac{1.17 \cdot K}{q_o A R}} \tag{31}$$

This last equation is equivalent to Eq. 23, when $\alpha = \frac{\pi}{2}$, being possible to obtain an approximated value of $I_m(\frac{\pi}{2})$ as

$$I_m(\frac{\pi}{2}) \approx I_m^* = \frac{1}{4} \sqrt[m]{\frac{1.17}{2}} \tag{32}$$

In order to check the similarity between (24) and (32), next Fig. 8 compares both expression for different values of m parameter. Approximated expression understimates the analytical approach in a range from 19% to 33% for a range of typical values of m parameter for superplastic applications between 0.3 and 0.7.

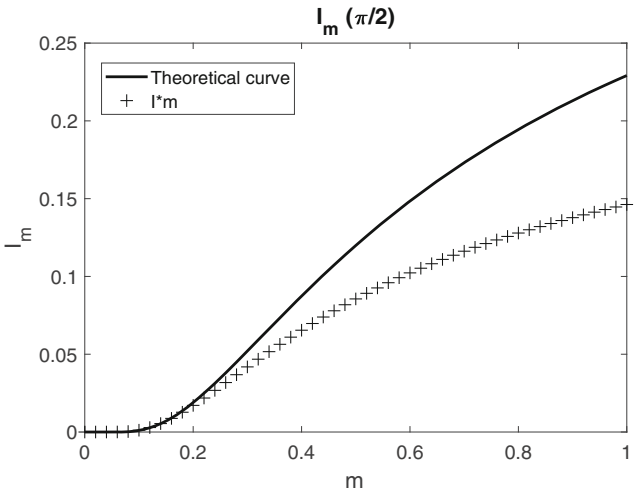

Fig. 8 Theoretical and approximated curves of I_m, Eqs. 24 and 32 respectively, as a function of m parameter

In order to deeply understand the use and the potentiality of this procedure, an independent FBF test is performed using Fig. 7. The test aims to get an estimated forming time for an specific external pressure, applied to a material and dimensionless parameters that are previously determined.

The independent test was performed on magnesium alloy AZ31, at constant pressure of 5 bars and 450^o. At these conditions, K and m parameters are estimated as 195 $MPas^m$ and 0.457 respectively by comparing experimental results [12] with numerical analysis. The sample AR is 22.5. Applying the expression (31) the estimated forming time was 362 s., meanwhile the experimental forming time was set in 422 s. This estimation provides an error of 14%. A study of the propagation of the uncertainties was also performed following the standard procedures [37] in order to determine the typical threshold for error in forming time. This study reveals that experimental errors from material characterisation (5%), pressure level (0.25%) and geometrical variations (1%) can provide forming time errors (ϵ_r) in the order of 20%, see Table 1. Thus, forming time errors lower than 20% can be considered as good estimations.

Alternatively, the same procedure can be applied in order to get an estimation of the necessary external pressure, q_o, to obtain an specific strain rate at the apex dome.

$$q_o \approx \frac{1.17 \cdot \sigma_o(\dot{\varepsilon}_o)}{AR} \tag{33}$$

Conclusions

Following the procedure of [11], a dimensional analysis of a SPF process has been developed. The study has been focused on the forming time of FBF tests as an output parameter. Dimensionless parameters have been obtained through a normalization procedure of the physical equations, using the density as a mass variable. However, the density does not seem a proper variable for defining the material since the inertial forces of the process have been proved to be much lower than the stress forces. In that sense, further research is needed in order to use a distinct mass variable linked to the stress forces to allow a better characterisation of the material. Dimensionless parameter κ_5 has been used as a forming time estimator that matches with the analytical expressions. This ratio between pressure and material stress is directly related to the aspect ratio of the sample and let us write the forming time as a simple expression of material parameters (K, m), external pressure and geometrical dimensions. In this way, DA has been used to study free-bulge tests as a first step to integrate DA in initial stages of the SPF process layout. Future works can be conducted aiming to prove the availability of down-scale tests and the use of equivalent materials.

Acknowledgements The authors wish to thank Prof. Luigi Tricarico, Prof. Donato Sorgente and the Dipartimento di Meccanica, Matematica e Management (DMMM) of the University of Bari (Italy) for allowing to perform the tests in its facilities.

Compliance with Ethical Standards

Conflict of interests The authors declare that they have no conflict of interest.

References

1. Alabort E, Putman D, Reed RC (2015) Acta Mater 95:428. https://doi.org/10.1016/j.actamat.2015.04.056
2. Ghosh AK, Hamilton CH (1986) Def Sci J 36(2):153. https://doi.org/10.1016/B978-1-84569-753-2.50010-8
3. Hefti L (2007) J Mater Eng Perform 16(2):136. https://doi.org/10.1007/s11665-007-9023-5
4. Boyer R (1996) Mater Sci Eng A 213(1-2):103. https://doi.org/10.1016/0921-5093(96)10233-1
5. Barnes AJ (2007) J Mater Eng Perform 16(4):440. https://doi.org/10.1007/s11665-007-9076-5. http://link.springer.com/10.1007/s11665-007-9076-5
6. Hefti L (2004) J Mater Eng Perform 13:678. https://doi.org/10.1361/10599490421286
7. Jovane F (1968) Int J Mech Sci 10:403
8. Majidi O, Jahazi M, Bombardier N (2018;2019) Int. J. Material Forming 12(4):693
9. ASTM (2011) E2448-11: standard test method for determining the superplastic properties of metallic sheet materials (ASTM)
10. ASTM (2015) E2712-15: standard test methods for bulge-forming superplastic metallic sheet (ASTM)
11. Padmanabhan KA, Vasin RA, Enikeev FU (2001) Superplastic flow: phenomenology and mechanics. Springer, Berlin
12. Sorgente D, Palumbo G, Scintilla LD, Tricarico L (2016) Int J Adv Manuf Technol 83(5–8):861. https://doi.org/10.1007/s00170-015-7614-0
13. Aksenov SA, Chumachenko EN, Kolesnikov AV, Osipov SA (2015) J Mater Process Technol 217:158. https://doi.org/10.1016/j.jmatprotec.2014.11.015
14. Albakri M, Abu-Farha F, Khraisheh M (2013) Int J Mech Sci 66:55. https://doi.org/10.1016/j.ijmecsci.2012.10.008
15. Yoo JT, Yoon JH, Lee HS, Youn SK (2012) J Mech Sci Technol 26(7):2101. https://doi.org/10.1007/s12206-012-0523-3
16. Yoon JH, Yi YM, Lee HS (2012) Mater Werkst 43(9):805. https://doi.org/10.1002/mawe.201200046
17. Sorgente D, Tricarico L (2014) Int J Mater Form 7(2):179. https://doi.org/10.1007/s12289-012-1118-3
18. Jeyasingh JJV, Kothandaraman G, Sinha PP, Rao BN, Reddy AC (2008) Mater Sci Eng A 478(1-2):397. https://doi.org/10.1016/j.msea.2007.05.050
19. Franchitti S, Giuliano G, Palumbo G, Sorgente D, Tricarico L (2008) Int J Mater Form 1:1067. https://doi.org/10.1007/s12289-008-0
20. Antoniswamy A, Taleff E, Hector L, Carter JT (2015) Mater Sci Eng A 631:1. https://doi.org/10.1016/j.msea.2015.02.018
21. Carpenter A, Antoniswamy A, Carter JT, Hector L, Taleff E (2014) Acta Mater 68:254. https://doi.org/10.1016/j.actamat.2014.01.043
22. Jarrar FS, Abu-Farha F, Hector L, Khraisheh MK (2009) J Mater Eng Perform 18(7):863. https://doi.org/10.1007/s11665-008-9322-5
23. Pradeep S, Pancholi V (2014) Metallur Mater Trans A: Phys Metallur Mater Sci 45(13):6207. https://doi.org/10.1007/s11661-014-2573-x
24. Barenblatt GI (1996) Scaling, self-similarity, and intermediate asymptotics: dimensional analysis and intermediate asymptotics. Cambridge texts in applied mathematics. Cambridge University Press. https://doi.org/10.1017/CBO9781107050242
25. Aksenov SA, Sorgente D (2017) Procedia Eng 207:1892
26. Majidi O, Jahazi M, Bombardier N (2019) Int J Adv Manuf Technol 102(5):2357
27. Buckingham E (1914) Phys Rev (Series) I:4. https://doi.org/10.1103/physrev.4.345
28. Belk JA (1975) Int J Mech Sci 17(8):505. https://doi.org/10.1016/0020-7403(75)90015-6
29. Guo ZX, Ridley N (1989) Mater Sci Eng A 114(C):97. https://doi.org/10.1016/0921-5093(89)90849-6
30. Enikeev FU, Kruglov AA (1995) Int J Mech Sci 37(5):473
31. Giuliano G, Franchitti S (2007) Int J Mach Tools Manuf 47(3-4):471. https://doi.org/10.1016/j.ijmachtools.2006.06.009
32. Ingelbrecht C (1985) Superplastic deformation of titanium. University of Surrey, Ph.D. thesis
33. Taleff E, Hector LG Jr, Verma R, Krajewski PE, Chang JK (2010) J Mater Eng Perform 19(4):488
34. Yu-quan S, Jun Z (1986) Mater Sci Eng 84:111
35. Ramos RE, Prada JCG, Giuliano G (2011) Análisis de las características mecánicas de la superplasticidad: aplicación a la aleación de PbSn60 (in Spanish). Ph.D. thesis
36. Sorgente D, Palumbo G, Piccininni A, Guglielmi P, Tricarico L (2017) Int J Adv Manuf Technol, 90(1-4). https://doi.org/10.1007/s00170-016-9235-7
37. Fornasini P (2009;2008) The uncertainty in physical measurements: an introduction to data analysis in the physics laboratory, 1st edn. Springer, New York